Express Polymer Letters Vol.16, No.8 (2022) 786–797
Available online at www.expresspolymlett.com
https://doi.org/10.3144/expresspolymlett.2022.58

Research article

A novel ammonia sensor based on cellulose/graphene oxide functionalized with ethylenediamine

Sawsan Dacrory[1], *Ahmed M. Saeed*[2], *Ragab E. Abouzeid*[1*]

[1]Cellulose and Paper Department, National Research Centre, 12622 Giza, Egypt
[2]Chemistry Department, Faculty of Science, Al-Azhar University, Cairo, Egypt

Received 18 November 2021; accepted in revised form 5 April 2022

Abstract. In this study eco-friendly cellulose/graphene oxide scaffold has been formulated in the presence of different ratios of ethylenediamine (EDA) as a crosslinker via a lyophilization instrument. Cellulose was extracted from paper wastes and companied with graphene oxide (GO). Chemical structure and surface morphology of the extracted cellulose and cellulose/GO foam were investigated by infrared spectroscopy (FTIR), X-ray diffraction (XRD), thermal gravimetric analysis (TGA), and the scanning electron microscope (SEM) techniques. The prepared cellulose/GO foam was used as a gas sensing material, including the sensitivity and response/recovery times toward NH_3 vapor. The cellulose/GO cryogel which was prepared with the addition of 1.5 mmol of EDA showed the highest sensitivity at room temperature with the response and recovery times at 490 and 620 s, respectively, compared to the cryogel prepared with 2.25 mmol EDA and the pristine cellulose cryogel.

Keywords: *smart polymers, cellulose, paper waste, NH_3 gas capture, graphene oxide (GO)*

1. Introduction

Environmental pollution from various gases generated from various sources is a big burden. Because of its colorlessness and toxicity, ammonia is one of the most dangerous gases [1]. It is also used for a variety of industrial and home purposes, including compound fertilizer, synthetic fiber, and biofuel. Furthermore, a large dose of ammonia can have negative consequences on the human body, such as eye discomfort, sore throat, skin irritation, and respiratory system irritation [2]. Therefore, this leads scientists to develop gas capture devices that are cost-effective, biodegradable, high sensitivity, and easy to detect [3]. Different material systems have been developed for the estimation of ammonia, such as graphene/polyaniline composite, reduced graphene oxide (RGO) [4], and thin films prepared from copper bromide [5], zinc oxide [6], and polypyrrole–graphene [7]. Among these materials systems, aerogel is the most attractive system that can be used due to its lightweight and porous structure. Aerogel is a 3D structure that can be fabricated from different materials; cellulose is a wildly used material due to its biodegradability, inexpensive, and non-toxic properties [8]. Due to increase the technological innovations, a variety of solid wastes has been produced. Among these solid wastes, millions of tons of paper are produced and used worldwide [9]. There has been a significant amount of paper waste (PW) generated as a result of numerous industrial activities, which has caused significant damage to the environment. So in recent years, there has been a considerable push to encourage ecologically friendly garbage management practices [10–12]. This waste consists of cotton or wood pulp composed of 90–99% cellulose fibers [13]. The use of naturally occurring and environmentally friendly

*Corresponding author, e-mail: r_abouzeid2002@yahoo.com

polymeric materials, such as cellulose, for producing composite materials for various purposes is receiving a lot of interest [14–18]. Cellulose is a major biopolymer, widespread and affordable on Earth. In recent years several studies have addressed various applications of compounds formed on the basis of cellulose fibers [19, 20]. These materials are promising in electronics applications such as gas sensors, bio-sensing, solar cells, optical detection, and power devices [1, 21–23]. Nanomaterials are considered a promising material for gas sensing due to their remarkable properties, large surface area, biodegradability, and high sensitivity [2]. Graphene oxide (GO) is a promising material that has a unique structure. It is composed of a single layer of graphene that has multi-function groups of carboxyl, hydroxyl, and epoxy groups. Attributed to its sp^2 hybridized and 2D hexagonal structure, GO is widely used as a gas sensor [24, 25]. Improving the gas sensing performance of cellulosic materials has been studied through combinations with several materials such as zinc oxide (ZnO), titanium dioxide (TiO_2), iron (III) oxide (Fe_2O_3), oxides of zirconium (ZrO_2), copper (Cu_2O and CuO), and graphene oxide (GO) [26–29].

In particular, most of the publications are concerned with the development of graphene-like materials, such as graphene, graphene oxide, and reduced graphene oxide, for use in the production of sensors [30, 31]. SnO_2 and CuO nanoflower–decorated graphene sensors developed by Zhang *et al*. [32] had a maximum response of 4.9 percent to 300 ppm of NH_3. Because of its strong adsorption ability and the ability to enhance textural qualities by reducing it, graphite oxide may be successfully employed for room-temperature detection of ammonia. However, the data on graphite oxide's application as an active material for ammonia gas sensors in its initial non-reduced state is inadequately reported, and the research is mainly focused on graphene oxide sheets or reduced graphene oxide [33–35]. To our knowledge, there are no previous studies of the fabrication of cellulose graphene oxide foam as an ammonia sensor. So, herein, we present a cheap, simple, eco-friendly and biodegradable, reusable, portable, highly sensitive, and real-time detection for ammonia gas sensor based on cellulose/GO foam in the presence of ethylenediamine (EDA) as a crosslinker via the freeze-drying process. Extracted cellulose, GO, and cellulose/GO foam have been characterized by FTIR, SEM, XRD, and TGA instruments. In addition, the gas-sensing properties were studied by measuring the resistance changes under exposure to the ammonia gas.

2. Materials and methods

Graphite (G) powder (99.9%) was purchased from Fisher Scientific (United Kingdom). Potassium permanganate (>99%) and hydrogen peroxide (30%) were bought from Bio Basic Canada Inc. (Canada) and Carl Roth GmbH (Germany), respectively. Ethylenediamine (EDA), ammonia, and sodium chlorite were purchased from Loba Chem (India).

2.1. Extraction of cellulose from paper waste (PW)

The PW biomass was collected from old used books, notes, and copying papers. Paper pulp was prepared from PW (100 g) by cutting it into small pieces and soaking it in hot water. In order to remove hemicellulose, resin, and lignin, we soaked the pulp in sodium hydroxide (20%) for 1 hour at 70 °C before drying it [13]. Then paper pulp was bleached with sodium chlorite at 70 °C for 1 h in an acidic medium. The pure white extracted cellulose was washed and dried at room temperature for further utilization [36].

2.2. Preparation of GO

GO nanosheet was prepared through the modified Hummer's method as described in previous work [37]. Briefly, 27 ml of sulfuric acid (H_2SO_4) and 3 ml of phosphoric acid (H_3PO_4) were mixed and stirred for several minutes. Then 0.225 g of graphite powder was added. 1.32 g of potassium permanganate ($KMnO_4$) was added slowly into the solution. The mixture was allowed to stir for 6 h until the solution became dark green. 0.675 ml of hydrogen peroxide (H_2O_2) was dropped slowly and stirred for 10 minutes to remove the excess $KMnO_4$. After that, 10 ml of hydrochloric acid (HCl) and 30 ml of deionized water (DIW) were added. Then, the supernatant was decanted away and rewashed DIW 3 times. The black product of GO was dried using the oven at 90 °C for 24 h [38].

2.3. Preparation of cellulose/GO foam

In a 250 ml beaker, 1 g of the extracted cellulose was dispersed in 30 ml DIW. Then 0.1 g GO was sonicated for 2 min and added to cellulose solution. Different ratios of ethylenediamine (1.5, and 2.25 mmol) were added. A homogenous solution is obtained by homogenizer for 5 min. The precursors are placed

in a refrigerator at –18 °C for more than 24 h. The cellulose/GOcryogels are obtained by a freeze-drying process using an Alpha 1–2 LDPlus, freeze-dryer, Martin Christ Gefriertrocknungsanlagen GmbH (Germany) [1, 39].

2.4. Characterizations

FTIR spectra were measured using a Shimadzu FTIR Spectrophotometer (8007S) (UniCam Ltd., UK). The XRD patterns were investigated on a Diano X-ray diffractometer using CuKα radiation source energized at 45 kV and an X-ray diffractometer (PW 1930 generator, PW 1820 goniometer, Philips (The Netherlands)) with CuK radiation source (λ = 0.15418 nm), at a diffraction angle range of 2θ from 10 to 70° in reflection mode. The surface morphology was analyzed using a FEI-Quanta 200 FEG-ESEM (The Netherlands) scanning electron microscope (SEM), environmental scanning without coating. With a JEOL JEM-2100, Jeol Ltd. (Japan) transmission electron microscope (TEM) at 100 000× magnification and an acceleration voltage of 120 kV, the image of the GO was obtained. An STA6000, Perkin Elmer (USA) TGA was used to test the thermal stability (10 °C/min). Temperatures ranged between room temperature and 800 °C under a nitrogen atmosphere.

2.5. Gas sensing measurements

The gas-sensing properties were elucidated by measuring the resistance changes under exposure to the target gas. For this purpose, 1 cm × 2 cm cryogel-samples were cut and used for NH_3 vapor sensing. A homemade static gas sensing testing system including a pyrex round (of 2 l volume) and areal-time voltage acquisition platform using a programmable digital multimeter interfaced with a laptop. The sensing measurements were accomplished according to Habib *et al.* [40]. Briefly, 5 V bias voltage was applied to the sensor circuit using a DC power supply and a load resistance (R_L) was connected with the sensor to measure the sensor output signal and the resistance of the sensors was measured using the data obtained by the multimeter (Figure 1). The relative humidity (*RH*) and temperature were ~40%, and ~25 °C, respectively. NH_3 was the target gas by injection of the liquid NH_3 (25%) using a pipette (1 ml) on an evaporator to be converted to vapors [41]. The concentrations of NH_3 gas were calculated according to Equation (1):

$$V_{NH_3} = 10^{-6} \cdot V_0 \cdot C_{NH_3} \quad (1)$$

where V_0 is the volume of the test round (2000 ml), V_{NH_3} [ml] is the required NH_3 volume, and C_{NH_3} is the concentration [ppm] of the NH_3 vapor. The gas response was calculated using R_a/R_g, where R_a and R_g are the sensor resistances in the air the target vapor, respectively. The response time is the time needed for R_g to be reduced to 90% of its initial value, while the recovery time is the time needed for the R_g to reach 90% of its initial value [42, 43].

3. Results and discussion

3.1. GO characterizations

XRD is a useful tool to study the chemical and physical changes of different compounds. Figure 2a shows the synthesized GO by modified Hummer's method of oxidation. The distinctive peak at 2θ = 26° in the graphite pattern disappeared, and a new characteristic

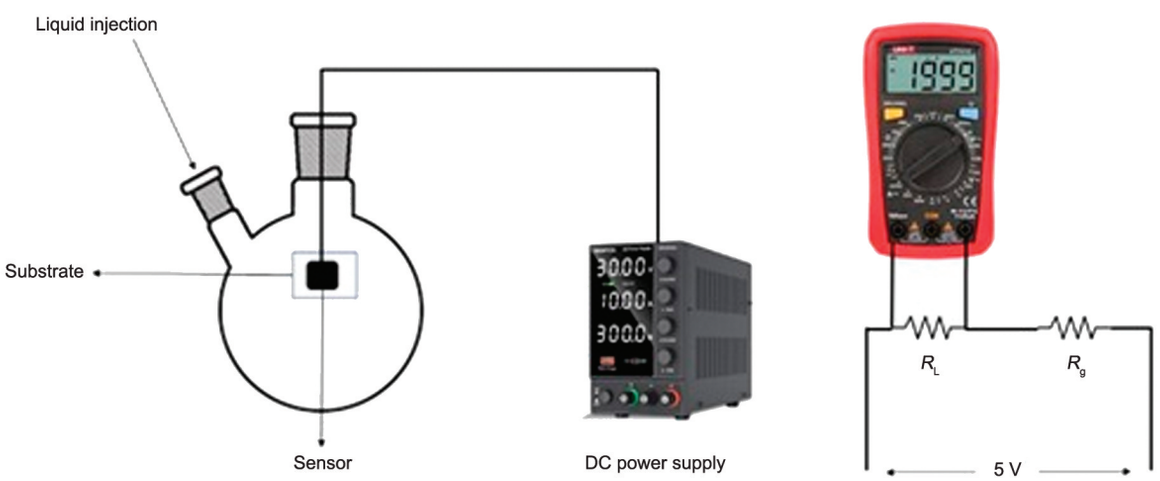

Figure 1. The experimental set-up of the gas sensing system.

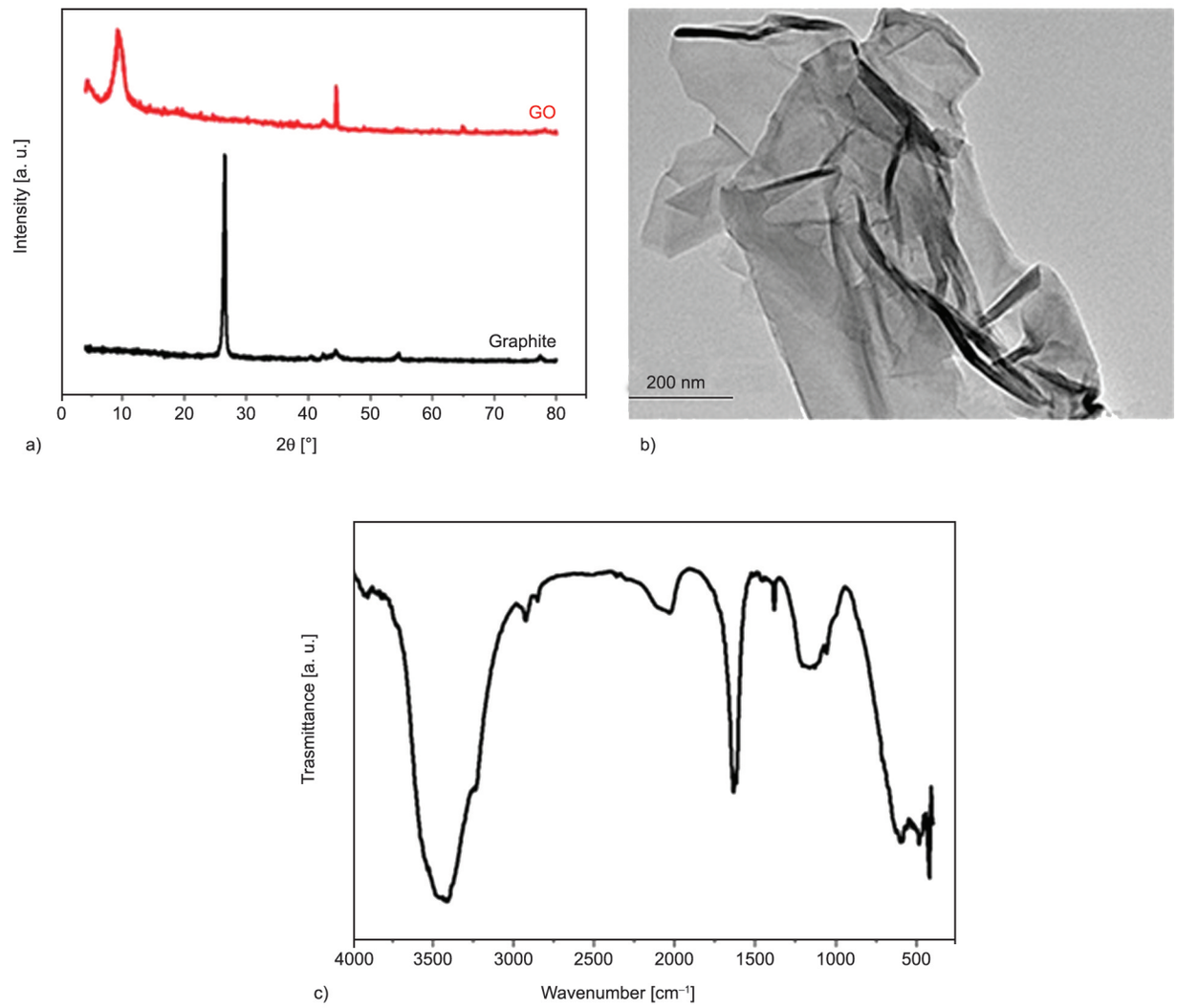

Figure 2. XRD (a), TEM (b) and (c) FTIR of GO.

peak at 2θ = 10° appears in the GO pattern due to new groups formation [38]. Two peaks were observed above 40° due to reflections from the used aluminum holder [44]. Figure 2b displays TEM of GO where irregular stacking of smooth surface of graphene sheets appears with different transparency areas. That indicates a much thinner sheet of GO [45, 46]. Figure 2c illustrates the FTIR of GO that shows different peaks of oxygen-derived species. The peaks at 3500 cm^{-1}assigned to OH carboxy, at 2900 cm^{-1} due to C–H, at 1600, and 700 cm^{-1} assigned to C=O and C=C respectively, as well the peak at 1100 cm^{-1} assigned to C–O [47, 48].

3.2. Preparation of cellulose/GO foam

Cellulose has extracted from the waste paper (WP) with an extraction efficiency of 76%. GO after sonication has been added to the extracted cellulose solution and cross-linked together by ethylenediamine (EDA) as in Figure 3a. FTIR analysis is a considerable tool used to investigate the chemical structure of compounds. Figure 3b shows the FTIR spectra of the extracted cellulose and cellulose/GO foam. FTIR spectra of cellulose show adsorption bands at 3500, 2900,1629, 1400 and 1040 cm^{-1} of OH stretching, CH stretching, absorbed water, crystallinity peak, and ether linkage C–O–C, respectively [49, 50]. While FTIR spectra of cellulose/GO foam represent a high abroad absorption peak of OH stretching and N–H of cellulose and EDA at 3500 $cm^{-1}$and, the intensity increased of the peak at 1620 cm^{-1} attributed to increasing amide group and C=O groups of GO and EDA. As well as the peak of crystallinity CH_2 of cellulose at 1400 cm^{-1} decreased due to GO incorporation [3, 51].

3.3. Scanning electron microscope (SEM)

The surface morphology of cellulose and cellulose/GO foam are given in Figures 4a and 4b That

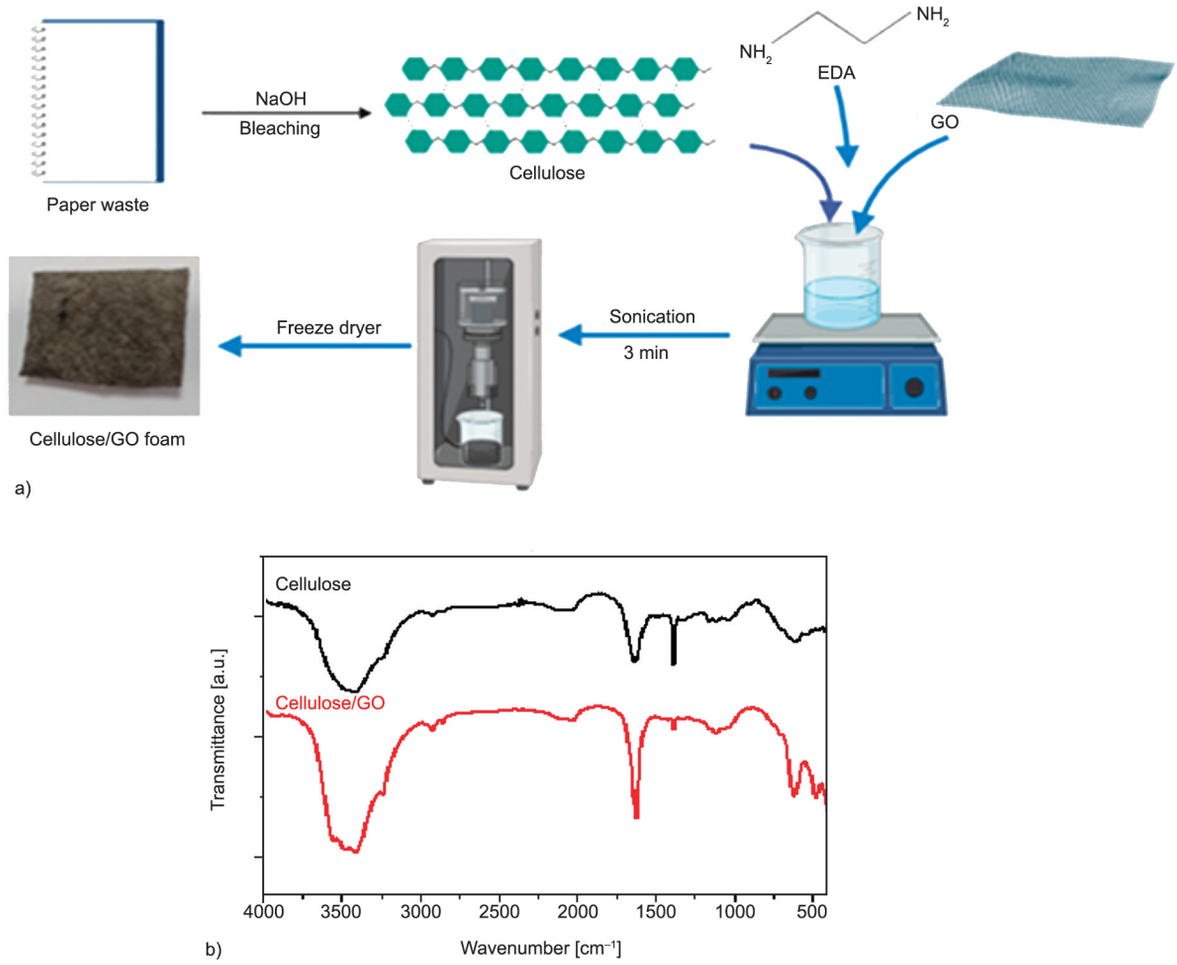

Figure 3. a) Preparation scheme of cellulose/GO foam and b) FTIR of cellulose and cellulose/GO foam.

demonstrates the surface morphology of cellulose as a small long fiber. At the same time, cellulose/GO foam exhibits a foam-like structure. As well, the fibers are coated with GO with a large pore size. Figure 4c, 4d shows a smooth and homogenous white and black surface of cellulose and cellulose/GO, respectively.

3.4. X-ray diffraction

An X-ray diffractometer is a useful parameter to determine the crystal structure of as-prepared cellulose/GO foam. Figure 5 displays the XRD pattern of GO, cellulose, and cellulose/GO. As a result, GO includes a distinctive peak at 2θ = 10°. This peak completely disappears in cellulose/GO foam, and it may be due to the expected interaction between GO function groups and cellulose groups or due to the low concentration of GO in the prepared foam [37, 52, 53]. The cellulose pattern exhibits two broad peaks at 2θ = 15, 23° which are assigned to cellulose I [22, 54]. While in the cellulose/GO pattern, two overlapped peaks at2θ = 23° have appeared, and the peak at 2θ = 15° became small, which confirms the presence of cellulose II [46].

3.5. Thermogravimetric analysis (TGA)

The TGA thermogravimetric curves were evaluated and presented in Figure 6a. The thermal decomposition behavior of cellulose and cellulose/GO composite in a nitrogen atmosphere over the temperature range of 25–800 °C was studied. It can be seen from the graph in Figure 6a, that the decomposition behavior of cellulose and cellulose/GO composite is completely different. The weight loss that occurs in the first decomposition stage of cellulose takes place at the temperature of 200–350 °C due to the depolymerization with dehydration and the release of volatile compounds such as carbon dioxide, methanol, and acetic acid. This behavior is consistent with many results for cellulosic materials. The final yield was only 10% at 700 °C. The TGA of cellulose/GO composite, the weight-loss begins at 100 °C due to water evaporation from the adsorbed water. The weight

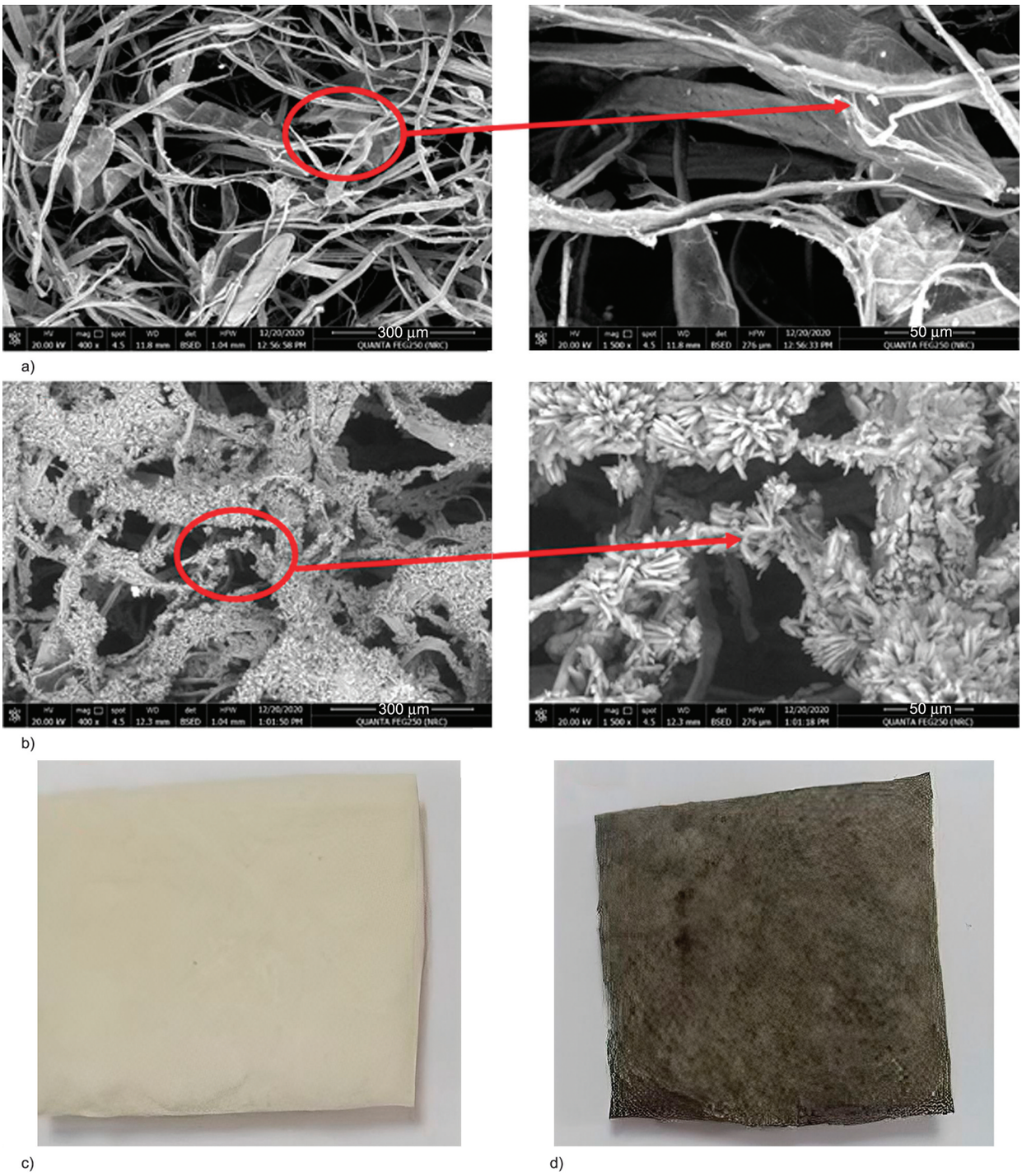

Figure 4. (a, b) SEM and (c, d) photographs of cellulose and cellulose/GO.

yield of the cellulose/GO composite is around 45% at 700 °C. This dramatic increase in the final weight yield of the composite compared to pure cellulose is due to the presence of graphene oxide and the cross-linked with EDA. Figure 6b shows DTG weight loss occurs through two stages for cellulose and in many stages for cellulose/GO. So this foam has a kind of stability due to its structure.

3.6. Sensing properties

Figure 7 shows the response of the prepared cryogels to different concentration of NH_3 at room temperature. The cellulose/GO cryogels exhibited good sensing characteristics toward NH_3 down to 5 ppm concentration. The resistance always decreased rapidly under exposure to NH_3 and recovered after exposing the sensor to air, indicating reversible response

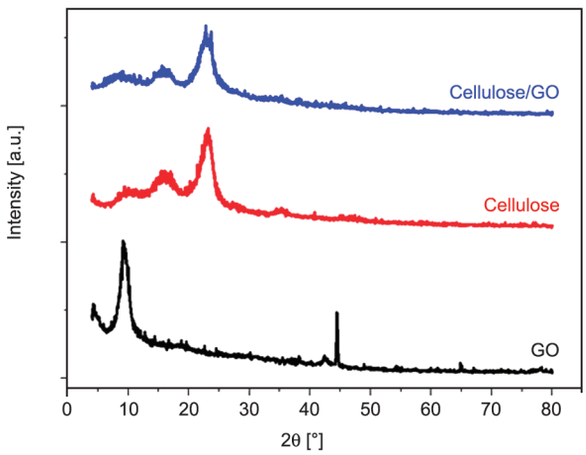

Figure 5. XRD of GO, cellulose and cellulose/GO foam.

characteristics. This response was higher than that of pristine cellulose cryogel (1.08, 3.35 and 6.67 and reached 17.1, 436.34 and 205.2 for cellulose, cellulose/GO with 1.5 mmol ethylenediamine (EDA) and cellulose/GO with 2.25 mmol EDA at 5 and 100 ppm of NH_3, respectively) due to the presence of GO which can adsorb gas molecules through the surface functional groups [25]. Moreover,the response values show nearly linear relationship with NH_3 vapor concentrations. Figure 8 represents the response as a function of time for the cellulose/GO cryogels prepared with addition of 1.5 and 2.25 mmol of EDA. As the concentration of NH_3 was increased, more molecules were adsorbed and the higher the response. On the other hand, the low response at lower NH_3 concentrations is due to the less NH_3 molecules adsorbed. Moreover, the response of the sample prepared with addition of 1.5 mmol EDA as a crosslinker exhibited higher response to NH_3 than the cellulose without GO and the sample with addition of 2.25 mmol EDA. Decreasing the available functional groups of GO may be the reason because ofthe consumption ofthe GO carboxyl groups by the reaction with EDA [3]. In addition, due to low permeability of GO for most gases [55], it is expected to tune the gas permeation of the cellulose matrix, by increasing the amount of EDA the functional groups on GO will decreased leading to the residual NH_3 vapor may pass through the porous network structure of the cellulose matrix leading to gas permeate problem.

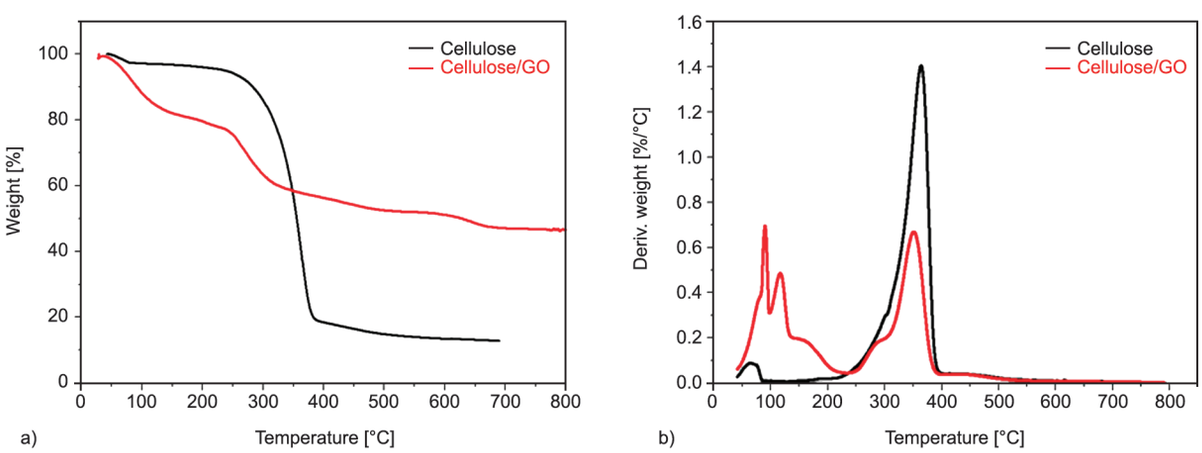

Figure 6. a) TGA and b) DTG of cellulose and cellulose/GO foam.

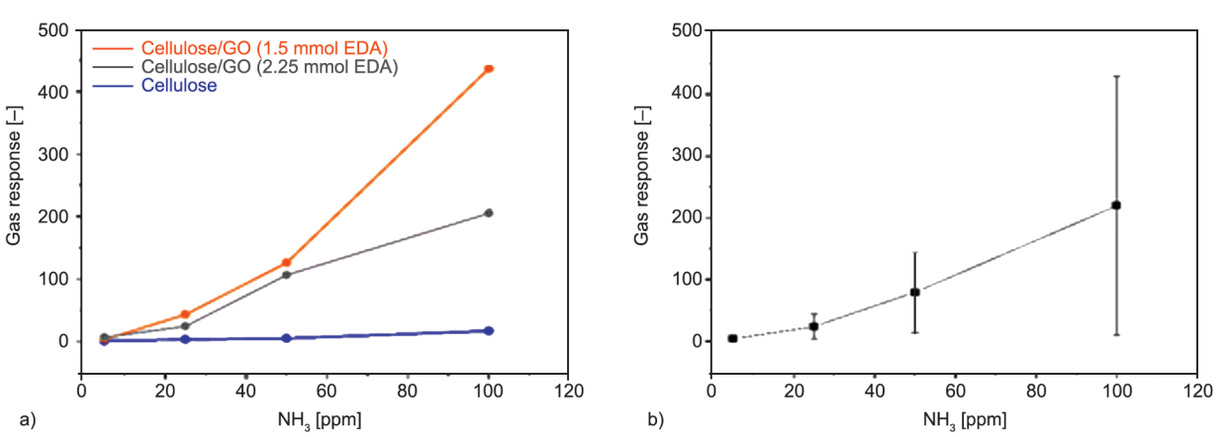

Figure 7. Gas response of the cryogels for various NH_3 concentrations (a). The error bars denote the standard deviation of the mean values of the responses obtained from three cryogel sensors (b).

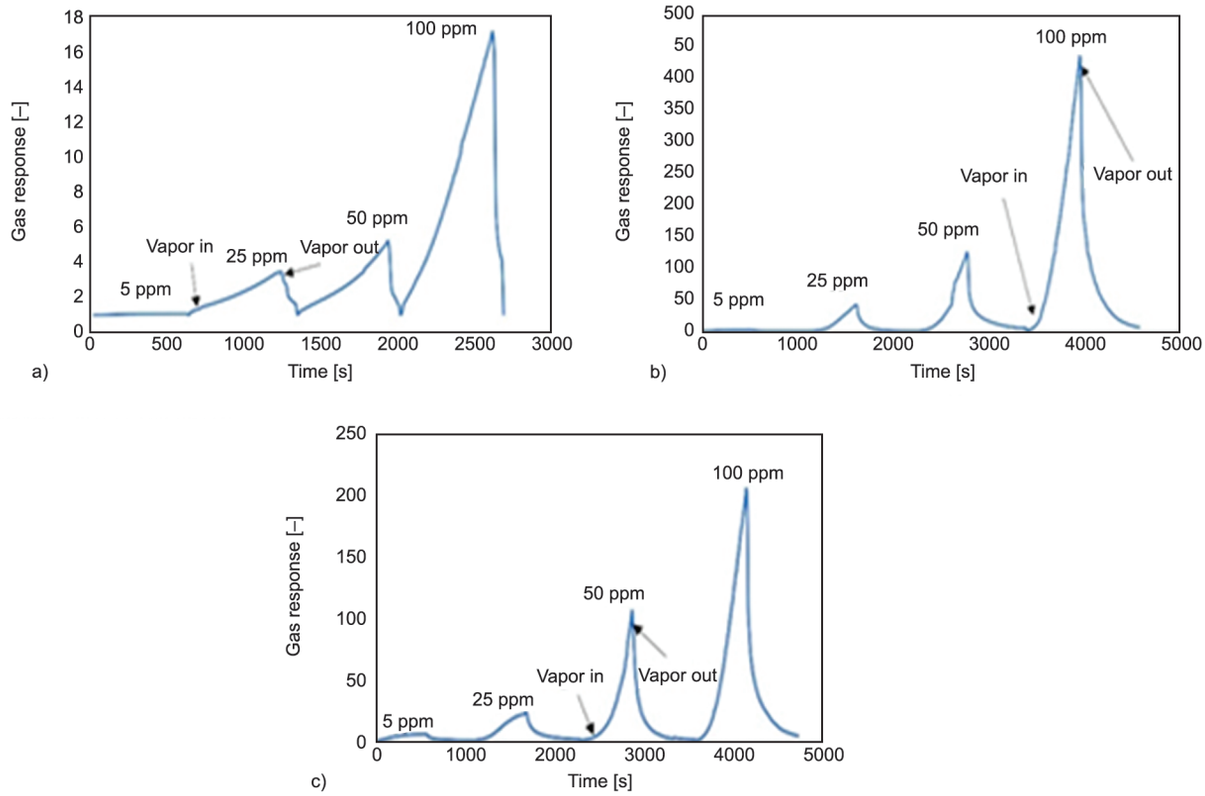

Figure 8. Gas responses of a) cellulose, b) cellulose/GO (1.5 mmol EDA) and c) cellulose/GO (2.25 mmol EDA) to different concentrations of NH_3.

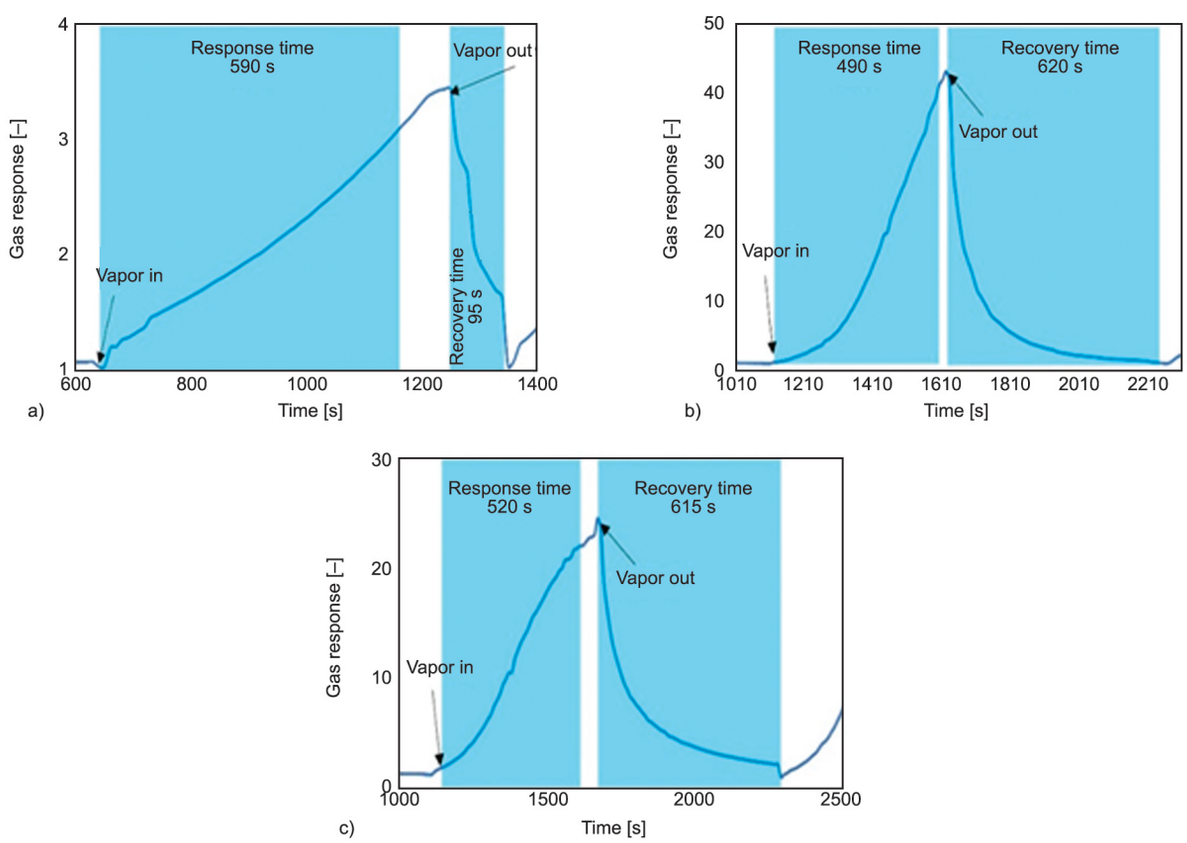

Figure 9. The dynamic response curve of a) cellulose, b) cellulose/GO (1.5 mmol EDA) and c) cellulose/GO (2.25 mmol EDA) toward 25 ppm NH_3.

Therefore, less crosslinker (EDA) amount make cellulose/GO cryogel exhibits better sensor performance [56]. Additionally, since the cellulose matrix has open-porous structure as well as large surface area and many vapor channels, so that, their swelling and de-swelling in addition to the adsorption and desorption of the vapor molecules on the GO are fast and effective. Therefore, at higher EDA amount (as in cellulose/GO cryogel with 2.25 mmol EDA), the network becomes denser and destroying the conductive network requires larger swelling which finally leading to lower response [57].

The response and recovery times of the prepared cryogels are depicted in Figure 9. The response/recovery times were 490 s/620 s and 520 s/615 s for cryogel with1.5 mmol and 2.25 mmol EDA, respectively. The sample with the addition of 1.5 mmol EDA, which has the highest response, recorded the fastest response time. The response time is good, but the recovery time is longer compared to cellulose without GO (Figure 9a), since the adsorbed gas molecules are chemically and physically adsorbed on GO [25] and must be desorbed entirely from the inner layers of the sensing material [58].

4. Conclusions

This work demonstrates the possibility of utilizing cellulose/GO composite cryogels as NH_3 vapor sensors. These cryogels exhibit fast response and good recovery times in addition to high sensitivity. A nearly linear response was obtained in a wide range of NH_3 vapor concentrations; therefore, cellulose/GO cryogels may be used for vapor quantification. The sensitivity of these composite cryogels was affected by the amount of EDA, which reduces the capacity of GO for adsorption of the NH_3 vapor. Thus, the response of the cellulose/GO prepared with less EDA was higher than other cryogels. Finally, by combining the highly open-porous cellulose matrix from paper wastes with GO, cellulose/GO cryogels may be utilized as green, inexpensive, and scalable sensing materials.

Acknowledgements

The authors would like to acknowledge the financial support for this research from National Research Centre.

References

[1] Khattab T. A., Dacrory S., Abou-Yousef H., Kamel S.: Development of microporous cellulose-based smart xerogel reversible sensor *via* freeze drying for naked-eye detection of ammonia gas. Carbohydrate Polymers, **210**, 196–203 (2019). https://doi.org/10.1016/j.carbpol.2019.01.067

[2] Karaduman I., Er E., Çelikkan H., Erk N., Acar S.: Room-temperature ammonia gas sensor based on reduced graphene oxide nanocomposites decorated by Ag, Au and Pt nanoparticles. Alloys and Compounds, **722**, 569–578 (2017). https://doi.org/10.1016/j.jallcom.2017.06.152

[3] Zhou F., Tien H. N., Dong Q., Xu W. L, Li H., Li S., Yu M.: Ultrathin, ethylenediamine-functionalized graphene oxide membranes on hollow fibers for CO_2 capture. Membrane Science, **573**, 184–191 (2019). https://doi.org/10.1016/j.memsci.2018.11.080

[4] Ghosh R., Singh A., Santra S., Ray S. K., Chandra A., Guha P. K.: Highly sensitive large-area multi-layered graphene-based flexible ammonia sensor. Sensors and Actuators B: Chemical, **205**, 67–73 (2014). https://doi.org/10.1016/j.snb.2014.08.044

[5] Bendahan M., Jacolin C., Lauque P., Seguin J-L., Knauth P.: Morphology, electrical conductivity, and reactivity of mixed conductor cubr films: Development of a new ammonia gas detector. The Journal of Physical Chemistry B, **105**, 8327–8333 (2001). https://doi.org/10.1021/jp010466j

[6] Chatterjee B., Bandyopadhyay A.: Development of zinc oxide sensors for detecting ammonia gas in the ambient air: A critical short review. Environmental Quality Management, **26**, 89–105 (2016). https://doi.org/10.1002/tqem.21483

[7] Xiang C., Jiang D., Zou Y., Chu H., Qiu S., Zhang H., Xu F., Sun L., Zheng L.: Ammonia sensor based on polypyrrole-graphene nanocomposite decorated with titania nanoparticles. Ceramics International, **41**, 6432–6438 (2015). https://doi.org/10.1016/j.ceramint.2015.01.081

[8] Dacrory S., Abou-Yousef H., Kamel S., Turky G.: Development of biodegradable semiconducting foam based on micro-fibrillated cellulose/Cu-NPs. International Journal of Biological Macromolecules, **132**, 351–359 (2019). https://doi.org/10.1016/j.ijbiomac.2019.03.156

[9] Joshi G., Naithani S., Varshney V. K., Bisht S. S., Rana V.: Potential use of waste paper for the synthesis of cyanoethyl cellulose: A cleaner production approach towards sustainable environment management. Journal of Cleaner Production, **142**, 3759–3768 (2017). https://doi.org/10.1016/j.jclepro.2016.10.089

[10] Al Kiey S. A., Hasanin M. S., Dacrory S.: Potential anticorrosive performance of green and sustainable inhibitor based on cellulose derivatives for carbon steel. Journal of Molecular Liquids, **338**, 116604 (2021). https://doi.org/10.1016/j.molliq.2021.116604

[11] Pivnenko K., Eriksson E., Astrup T. F.: Waste paper for recycling: Overview and identification of potentially critical substances. Waste Management, **45**, 134–142 (2014).
https://doi.org/10.1016/j.wasman.2015.02.028

[12] Hassan M., Berglund L., Abou-Zeid R., Hassan E., Abou-Elseoud W., Oksman K.: Nanocomposite film based on cellulose acetate and lignin-rich rice straw nanofibers. Materials, **12**, 595 (2019).
https://doi.org/10.3390/ma12040595

[13] Ghodake G. S., Yang J., Shinde S. S., Mistry B. M., Kim D-Y., Sung J-S., Kadam A. A.: Paper waste extracted α-cellulose fibers super-magnetized and chitosan-functionalized for covalent laccase immobilization. Bioresource Technology, **261**, 420–427 (2018).
https://doi.org/10.1016/j.biortech.2018.04.051

[14] Abouzeid R. E., Khiari R., El-Wakil N., Dufresne A.: Current state and new trends in the use of cellulose nanomaterials for wastewater treatment. Biomacromolecules, **20**, 573–597 (2019).
https://doi.org/10.1021/acs.biomac.8b00839

[15] Hassan M. L., Fadel S. M., Abouzeid R. E., Abou Elseoud W. S., Hassan E. A., Berglund L., Oksman K.: Water purification ultrafiltration membranes using nanofibers from unbleached and bleached rice straw. Scientific Reports, **10**, 11278 (2020).
https://doi.org/10.1038/s41598-020-67909-3

[16] Abouzeid R. E., Khiari R., Beneventi D., Dufresne A.: Biomimetic mineralization of three-dimensional printed alginate/TEMPO-oxidized cellulose nanofibril scaffolds for bone tissue engineering. Biomacromolecules, **19**, 4442–4452 (2018).
https://doi.org/10.1021/acs.biomac.8b01325

[17] Mousa H. M., Fahmy H. S., Abouzeid R., Abdel-Jaber G. T., Ali W. Y.: Polyvinylidene fluoride-cellulose nanocrystals hybrid nanofiber membrane for energy harvesting and oil-water separation applications. Materials Letters, **306**, 130965 (2022).
https://doi.org/10.1016/j.matlet.2021.130965

[18] Abou-Zeid R. E., Salama A., Al-Ahmed Z. A., Awwad N. S., Youssef M. A.: Carboxylated cellulose nanofibers as a novel efficient adsorbent for water purification. Cellulose Chemistry and Technology, **54**, 237–245 (2020).
https://doi.org/10.35812/CelluloseChemTechnol.2020.54.25

[19] Abou-Yousef H., Dacrory S., Hasanin M., Saber E., Kamel S.: Biocompatible hydrogel based on aldehyde-functionalized cellulose and chitosan for potential control drug release. Sustainable Chemistry and Pharmacy, **21**, 100419 (2021).
https://doi.org/10.1016/j.scp.2021.100419

[20] Vaezi K., Asadpour G., Sharifi H.: Effect of ZnO nanoparticles on the mechanical, barrier and optical properties of thermoplastic cationic starch/montmorillonite biodegradable films. International Journal of Biological Macromolecules, **124**, 519–529 (2019).
https://doi.org/10.1016/j.ijbiomac.2018.11.142

[21] Chu S., Yang L., Guo X., Dong L, Chen X., Li Y., Mu X.: The influence of pore structure and Si/Al ratio of HZSM-5 zeolites on the product distributions of α-cellulose hydrolysis. Molecular Catalysis, **445**, 240–247 (2018).
https://doi.org/10.1016/j.mcat.2017.11.032

[22] Dacrory S., Moussa M., Turky G., Kamel S.: *In situ* synthesis of Fe_3O_4@ cyanoethyl cellulose composite as antimicrobial and semiconducting film. Carbohydrate Polymers, **236**, 116032 (2020).
https://doi.org/10.1016/j.carbpol.2020.116032

[23] Prasetyo E. N., Semlitsch S., Nyanhongo G. S., Lemmouchi Y., Guebitz G. M.: Laccase functionalized cellulose acetate for the removal of toxic combustion products. Reactive and Functional Polymers, **97**, 12–18 (2015).
https://doi.org/10.1016/j.reactfunctpolym.2015.10.004

[24] Dacrory S., Hashem A. H., Hasanin M.: Synthesis of cellulose based amino acid functionalized nano-biocomplex: Characterization, antifungal activity, molecular docking and hemocompatibility. Environmental Nanotechnology, Monitoring and Management, **15**, 100453 (2021).
https://doi.org/10.1016/j.enmm.2021.100453

[25] Kumar R., Kumar A., Singh R., Kashyap R., Kumar R., Kumar D., Sharma S. K., Kumar M.: Room temperature ammonia gas sensor using meta toluic acid functionalized graphene oxide. Materials Chemistry and Physics, **240**, 121922 (2020).
https://doi.org/10.1016/j.matchemphys.2019.121922

[26] Poloju M., Jayababu N., Ramana Reddy M. V.: Improved gas sensing performance of Al doped ZnO/CuO nanocomposite based ammonia gas sensor. Materials Science and Engineering: B, **227**, 61–67 (2018).
https://doi.org/10.1016/j.mseb.2017.10.012

[27] Khan M. A. H., Rao M. V., Li Q.: Recent advances in electrochemical sensors for detecting toxic gases: NO_2, SO_2 and H_2S. Sensors, **19**, 905 (2019).
https://doi.org/10.3390/s19040905

[28] Li Z., Li H., Wu Z., Wang M., Luo J., Torun H., Hu P., Yang C., Grundmann M., Liu X., Fu Y.: Advances in designs and mechanisms of semiconducting metal oxide nanostructures for high-precision gas sensors operated at room temperature. Materials Horizons, **6**, 470–506 (2019).
https://doi.org/10.1039/C8MH01365A

[29] El-Gendy A., Abou-Zeid R. E., Salama A., Diab M. A-H. A-R., El-Sakhawy M.: TEMPO-oxidized cellulose nanofibers/polylactic acid/TiO_2 as antibacterial bionanocomposite for active packaging. Egyptian Journal of Chemistry, **60**, 1007–1014 (2017).
https://doi.org/10.21608/ejchem.2017.1835.1153

[30] Zhang H-B., Wang J-W., Yan Q., Zheng W-G, Chen C., Yu Z-Z.: Vacuum-assisted synthesis of graphene from thermal exfoliation and reduction of graphite oxide. Journal of Materials Chemistry, **21**, 5392–5397 (2011).
https://doi.org/10.1039/C1JM10099H

[31] Bourlinos A. B., Gournis D., Petridis D., Szabó T., Szeri A., Dékány I.: Graphite oxide: Chemical reduction to graphite and surface modification with primary aliphatic amines and amino acids. Langmuir, **19**, 6050–6055 (2003). https://doi.org/10.1021/la026525h

[32] Zhang D., Liu J., Jiang C., Liu A., Xia B.: Quantitative detection of formaldehyde and ammonia gas *via* metal oxide-modified graphene-based sensor array combining with neural network model. Sensors and Actuators B: Chemical, **240**, 55–65 (2017). https://doi.org/10.1016/j.snb.2016.08.085

[33] Basu S., Bhattacharyya P.: Recent developments on graphene and graphene oxide based solid state gas sensors. Sensors and Actuators B: Chemical, **173**, 1–21 (2012). https://doi.org/10.1016/j.snb.2012.07.092

[34] Hu N., Yang Z., Wang Y., Zhang L., Wang Y., Huang X., Wei H., Wei L., Zhang Y.: Ultrafast and sensitive room temperature NH_3 gas sensors based on chemically reduced graphene oxide. Nanotechnology, **25**, 025502 (2014). https://doi.org/10.1088/0957-4484/25/2/025502

[35] Seredych M., Tamashausky A. V., Bandosz T. J.: Graphite oxides obtained from porous graphite: The role of surface chemistry and texture in ammonia retention at ambient conditions. Advanced Functional Materials, **20**, 1670–1679 (2010). https://doi.org/10.1002/adfm.201000061

[36] Dacrory S., Abou-Yousef H., Abouzeid R. E., Kamel S., Abdel-aziz M. S., El-badry M.: Antimicrobial cellulosic hydrogel from olive oil industrial residue. International Journal of Biological Macromolecules, **117**, 179–188 (2018). https://doi.org/10.1016/j.ijbiomac.2018.05.179

[37] Dacrory S.: Antimicrobial activity, DFT calculations, and molecular docking of dialdehyde cellulose/graphene oxide film against Covid-19. Journal of Polymers and the Environment, **29**, 2248–2260 (2021). https://doi.org/10.1007/s10924-020-02039-5

[38] Ghanem A. F., Rehim M. H. A.: Assisted tip sonication approach for graphene synthesis in aqueous dispersion. Biomedicines, **6**, 63 (2018). https://doi.org/10.3390/biomedicines6020063

[39] Khattab T. A., Dacrory S., Abou-Yousef H., Kamel S.: Smart microfibrillated cellulose as swab sponge-like aerogel for real-time colorimetric naked-eye sweat monitoring. Talanta, **205**, 120166 (2019). https://doi.org/10.1016/j.talanta.2019.120166

[40] Habib I. Y., Tajuddin A. A., Noor H. A., Lim C. M., Mahadi A. H., Kumara N. T. R. N.: Enhanced carbon monoxide-sensing properties of chromium-doped ZnO nanostructures. Scientific Reports, **9**, 9207 (2019). https://doi.org/10.1038/s41598-019-45313-w

[41] Fan G., Chen D., Li T., Yi S., Ji H., Wang Y., Zhang Z., Shao G., Fan B., Wang H., Xu H., Lu H., Zhou Y., Zhang R., Sun J.: Enhanced room-temperature ammonia-sensing properties of polyaniline-modified WO_3 nanoplates derived *via* ultrasonic spray process. Sensors and Actuators B: Chemical, **312**, 127892 (2020). https://doi.org/10.1016/j.snb.2020.127892

[42] Chen Z., Lin Z., Xu M., Hong Y., Li N., Fu P., Chen Z.: Effect of gas sensing properties by Sn-Rh codoped ZnO nanosheets. Electronic Materials Letters, **12**, 343–349 (2016). https://doi.org/10.1007/s13391-016-6053-x

[43] Qiang X., Hu M., Zhao B., Qin Y., Zhang T., Zhou L., Liang J.: Preparation of porous silicon/Pd-loaded WO_3 nanowires for enhancement of ammonia sensing properties at room temperature. Materials Science in Semiconductor Processing, **79**, 113–118 (2018). https://doi.org/10.1016/j.mssp.2018.01.025

[44] Dacrory S., Abou Hammad A. B., El Nahrawy A. M., Abou-Yousef H., Kamel S.: Cyanoethyl cellulose/$BaTiO_3$/GO flexible films with electroconductive properties. ECS Journal of Solid State Science and Technology, **10**, 083004 (2021). https://doi.org/10.1149/2162-8777/ac1c56

[45] Stobinski L., Lesiak B., MalolepszyA., Mazurkiewicz M., Mierzwa B., Zemek J., Jiricek P., Bieloshapka I.: Graphene oxide and reduced graphene oxide studied by the XRD, TEM and electron spectroscopy methods. Journal of Electron Spectroscopy and Related Phenomena, **195**, 145–154 (2014). https://doi.org/10.1016/j.elspec.2014.07.003

[46] Lin W-D., Chang H-M., Wu R-J.: Applied novel sensing material graphene/polypyrrole for humidity sensor. Sensors and Actuators B: Chemical, **181**, 326–331 (2013). https://doi.org/10.1016/j.snb.2013.02.017

[47] Strankowski M., Włodarczyk D., Piszczyk Ł., Strankowska J.: Polyurethane nanocomposites containing reduced graphene oxide, FTIR, Raman, and XRD studies. Journal of Spectroscopy, **2**, 7520741 (2016). https://doi.org/10.1155/2016/7520741

[48] Sohail M., Saleem M., Ullah S., Saeed N., Afridi A., Khan M., Arif M.: Modified and improved Hummer's synthesis of graphene oxide for capacitors applications. Modern Electronic Materials, **3**, 110–116 (2017). https://doi.org/10.1016/j.moem.2017.07.002

[49] Mekheimer R. A., Hilmy N. M., Hameed A. A., Dacrory S., Sadek K. U.: Simple, three-component, highly efficient green synthesis of thiazolo[3,2-a]pyridine derivatives under neat conditions. Synthetic Communications, **41**, 2511–2516 (2011). https://doi.org/10.1080/00397911.2010.505700

[50] Mekheimer R. A., Abdelhameed A. M., Mohamed S. M., Sadek K. U.: Green, three component highly efficient synthesis of 2-amino-5,6,7,8-tetrahydro-4-H-chromen-3-carbonitriles in water at ambient temperature. Green Chemistry Letters and Reviews, **3**, 161–163 (2010).
https://doi.org/10.1080/17518251003619176

[51] Dacrory S.: Development of mesoporous foam based on dicarboxylic cellulose and graphene oxide for potential oil/water separation. Polymer Bulletin. in press (2022).
https://doi.org/10.1007/s00289-021-03963-9

[52] Wei X., Huang T., Yang J-H., Zhang N., Wang Y., Zhou Z-W.: Green synthesis of hybrid graphene oxide/microcrystalline cellulose aerogels and their use as superabsorbents. Journal of Hazardous Materials, **335**, 28–38 (2017).
https://doi.org/10.1016/j.jhazmat.2017.04.030

[53] Yadav M., Rhee K. Y., Jung I. H., Park S. J.: Eco-friendly synthesis, characterization and properties of a sodium carboxymethyl cellulose/graphene oxide nanocomposite film. Cellulose, **20**, 687–698 (2013).
https://doi.org/10.1007/s10570-012-9855-5

[54] Mahadeva S. K., Yun S., Kim J.: Flexible humidity and temperature sensor based on cellulose-polypyrrole nanocomposite. Sensors and Actuators A: Physical, **165**, 194–199 (2011).
https://doi.org/10.1016/j.sna.2010.10.018

[55] Joshi R. K., Carbone P., Wang F. C., Kravets V. G., Su Y., Grigorieva I. V., Wu H. A., Geim A. K., Nair R. R.: Precise and ultrafast molecular sieving through graphene oxide membranes. Science, **343**, 752–754 (2014).
https://doi.org/10.1126/science.1245711

[56] Zhang J., Jiang G., Goledzinowski M., Comeau F. J. E., Li K., Cumberland T., Lenos J., Xu P., Li M., Yu A., Chen Z.: Green solid electrolyte with cofunctionalized nanocellulose/graphene oxide interpenetrating network for electrochemical gas sensors. Small Methods, **1**, 1700237 (2017).
https://doi.org/10.1002/smtd.201700237

[57] Chen Y., Pötschke P., Pionteck J., Voit B., Qi H.: Aerogels based on reduced graphene oxide/cellulose composites: Preparation and vapour sensing abilities. Nanomaterials, **10**, 1729 (2020).
https://doi.org/10.3390/nano10091729

[58] Rani G. B., Saisri R., Kailasa S., Reddy M. S. B., Maseed H., Rao K. V.: Architectural tailoring of orthorhombic MoO_3 nanostructures toward efficient NO_2 gas sensing. Journal of Materials Science, **55**, 8109–8122 (2020).
https://doi.org/10.1007/s10853-020-04601-x